Charge transport in a double-stranded DNA: Effects of helical symmetry and long-range hopping

Sourav Kundu[1,*,†] and Constantinos Simserides[2,‡]

[1]*Department of Physics, GITAM University, Bengaluru Campus, Bengaluru - 561203, Karnatak, India*

[2]*National and Kapodistrian University of Athens, Department of Physics, Panepistimiopolis, Zografos, GR-15784, Athens, Greece*

(Received 14 June 2023; accepted 7 December 2023; published 8 January 2024)

Within a tight-binding framework, we examine conformation-dependent charge transport properties of the DNA double-helix, including helical symmetry and the possibility of multiple charge conduction pathways. Using techniques based on the Green's function method, we inspect changes in the localization properties of DNA in the presence of long-range hopping, with varying disorder strength. We study three characteristic DNA sequences, two periodic and one random. We observe that, in all cases, due to disorder-induced delocalization, the localization length variation is similar. We also investigate the effect of backbone energetics on current-voltage (I-V) responses, using the Landauer-Büttiker formalism. We find that, in the presence of helical symmetry and long-range hopping, due to environmental effects, DNA can undergo a phase transition from semiconductor to insulator.

DOI: 10.1103/PhysRevE.109.014401

I. INTRODUCTION

DNA, the basic building block of life, consists of four different nitrogenous bases: adenine (A), guanine (G), cytosine (C), and thymine (T), connected via hydrogen bonds in a ladder-like structure that is famously known as a double-helix [1]. Adenine (A) pairs with thymine (T) and guanine (G) pairs with cytosine (C). This is known as complementary base-pairing. The backbone structure of DNA is formed by phosphate groups and pentose sugars (deoxyriboses). Deoxyriboses are attached to the nitrogenous bases via similar C-N bonds. Most of the theoretical models consider charge conduction [2–9] through the π-π path between bases and no charge transport along the backbone sites. Even in cases of polaron hopping along DNA, the same mechanism was followed [10,11]. Considering energetic and spatial separation between sites, multiphonon-assisted hopping of small polarons between next-nearest neighbors was suggested as the transport mechanism responsible for the strong high-temperature dependence of the electrical conductivity in DNA [12]. In our present work, we model double-stranded DNA incorporating its helical symmetry and the presence of multiple conduction channels, as reported in a number of chirality-induced spin selectivity (CISS) studies [13–16].

We perform the following investigations, using three double-stranded (ds) DNA sequences: Two periodic, i.e., poly(dA)-poly(dT) and poly(dG)-poly(dC), as well as a random sequence containing both A-T and G-C base pairs. Random means that A-T and G-C base pairs are randomly organized over the DNA chain, with purine on purine: the sequence is generated via a random number generator in the range [0,1]; if the random number is less than 0.5, an A-T is inserted, otherwise a G-C. We model ds-DNA within the tight binding (TB) framework by incorporating helical symmetry into the widely used dangling backbone ladder model (DBLM) [17]. In a wire model [18,19], we have connections between successive base pairs which are the only sites included. In a ladder model [18], we have connections between bases of successive base pairs, hence the sites are the bases. If diagonal interactions are included, this is an extended ladder model [20]. If, to a wire model, we add interactions between base pairs and neighboring deoxyriboses (which are further connected to phosphate groups in the backbone), this is a fishbone wire model [18,21,22]. If, to a ladder model, we add interactions between bases and neighboring deoxyriboses (which are further connected to phosphate groups in the backbone), this is a fishbone ladder model [17,18] that can be found in the extended ladder version as well. The DBLM can also be called the fishbone ladder model. Some other TB variants are presented in Refs. [4,5,23,24].

Environmental fluctuations are modeled by varying the on-site energies of the backbone sites. In this article, first we check the density of states (DOS) profile of the three sequences for the clean case (without disorder). The term local density of states (LDOS) is often used to describe local variations of DOS, e.g., due to disorder or in small systems like molecules or oligomers, while, in periodic crystals of any dimensionality, DOS is, at least in some dimensions, continuous. We studied localization phenomena for all sequences, varying disorder strength and energy. Moreover, we investigated transmission profiles and plotted the transmission probability (T) versus energy (E) with varying disorder strength. Lastly, we studied the current-voltage (I-V) response of all sequences both for the clean case and also with disorder. We observed semiconductor-like cutoff in all cases. Lastly, we compare our model with DBLM and find that, due to the

*sourav.kunduphy@gmail.com

†SK does not have an affiliation at this time.

‡csimseri@phys.uoa.gr

presence of multiple conduction channels, charge transport along DNA gets enhanced in a significant manner.

This paper is organized in the following way. In Sec. II we lay down our theoretical formulation and describe the model Hamiltonian. We explain our numerical results in Sec. III and summarize our conclusions in Sec. IV.

II. THEORETICAL FORMULATION

The effective Hamiltonian for our model can be expressed as (for a schematic representation of this model we refer to Refs. [13,25])

$$H_{\rm DNA} = H_{\rm ladder} + H_{\rm backbone}, \tag{1}$$

where

$$H_{\rm ladder} = \sum_{j=I,II}\left[\sum_{i=1}^{N}\epsilon_{ij}c_{ij}^{\dagger}c_{ij} + \sum_{i=1}^{N-1}\sum_{n=1}^{N-n}(t_{nj}c_{ij}^{\dagger}c_{i+n,j} + \text{H.c.})\right] + \sum_{i=1}^{N} v(c_{iI}^{\dagger}c_{iII} + \text{H.c.}), \tag{2}$$

$$H_{\rm backbone} = \sum_{i=1}^{N}\sum_{j=I,II}\left(\epsilon_i^{q(j)}c_{iq(j)}^{\dagger}c_{iq(j)} + t_i^{q(j)}c_{ij}^{\dagger}c_{iq(j)} + \text{H.c.}\right), \tag{3}$$

where $c_{ij}^{\dagger}$ (c_{ij}) creates (annihilates) an electron at the ith site of the jth strand, t_{nj} represents the intrachain hopping integral between the sites n and $(n+i)$, and it becomes [16]

$$t_{nj} = t_{1j}e^{-(l_{nj}-l_{1j})/l_c}, \tag{4}$$

where t_{1j} is the nearest-neighbor hopping (NNH) strength, l_c is the decay constant, and l_{nj} measures the distance between the sites n and $(n+i)$. In terms of the radius R, stacking distance Δh and twisting angle $\Delta\phi$, we can write l_{nj} as [16]

$$l_{nj} = \sqrt{\left[2R\sin\left(\frac{i\Delta\phi}{2}\right)\right]^2 + (i\Delta h)^2}. \tag{5}$$

l_{nj} maps to the nearest-neighbor distance for $n = 1$ [25]. ϵ_{ij} is the on-site energy of nucleotides, $\epsilon_i^{q(j)}$ is the on-site energy of the backbone adjacent to the ith nucleotide of the jth strand, $t_i^{q(j)}$ is the hopping integral between a nucleotide and the corresponding backbone site, and v is the interstrand hopping integral. For simplicity, we set $\epsilon_i^{q(j)} = \epsilon_b$ and $t_i^{q(j)} = t_b$.

To explore the DNA transport properties, we use semi-infinite one-dimensional (1D) chains as source (S) and drain (D) electrodes connected to DNA at the left and right ends, respectively. The Hamiltonian of the entire system is given by

$$H = H_{\rm DNA} + H_{\rm S} + H_{\rm D} + H_{\rm tunneling}. \tag{6}$$

The explicit form of $H_{\rm S}$, $H_{\rm D}$, and $H_{\rm tunneling}$ are

$$H_{\rm S} = \sum_{i=-\infty}^{0}(\epsilon c_i^{\dagger}c_i + t c_{i+1}^{\dagger}c_i + \text{H.c.}), \tag{7}$$

$$H_{\rm D} = \sum_{i=N+1}^{\infty}(\epsilon c_i^{\dagger}c_i + t c_{i+1}^{\dagger}c_i + \text{H.c.}), \tag{8}$$

$$H_{\rm tunneling} = \tau(c_0^{\dagger}c_1 + c_N^{\dagger}c_{N+1} + \text{H.c.}), \tag{9}$$

where τ is the tunneling matrix element between DNA and the electrodes.

In this two-terminal setup, we use the Green's function approach to calculate the transmission probability $T(E)$ of electrons [26] through the DNA double-helix. The single-particle retarded Green's function operator representing the complete system, i.e., ds-DNA and two semi-infinite electrodes, at an energy E can be written as

$$G^{\rm r} = (E - H + i\eta)^{-1}, \tag{10}$$

where $\eta \to 0^+$ and H is the Hamiltonian of the entire system. Using the Fisher-Lee [26,27] relation, the two terminal transmission probability is defined as

$$T(E) = \text{Tr}[\Gamma_{\rm S}G^{\rm r}\Gamma_{\rm D}G^{\rm a}], \tag{11}$$

where E is the incident electron energy, $G^{\rm a}$ is the advanced Green's function operator, and Tr is the trace over the reduced Hilbert space spanned by the DNA molecule.

The effective Green's functions can be expressed in the reduced Hilbert space in terms of the self-energies of the source and drain electrodes

$$G^{\rm r} = [G^{\rm a}]^{\dagger} = \left[E - H_{\rm DNA} - \Sigma_S^{\rm r} - \Sigma_D^{\rm r} + i\eta\right]^{-1}, \tag{12}$$

where

$$\Sigma_{S(D)}^{\rm r(a)} = H_{\rm tunneling}^{\dagger}G_{S(D)}^{\rm r(a)}H_{\rm tunneling}, \tag{13}$$

and

$$\Gamma_{S(D)} = i\left[\Sigma_{S(D)}^{\rm r} - \Sigma_{S(D)}^{\rm a}\right]. \tag{14}$$

$G_{S(D)}^{\rm r(a)}$ being the retarded (advanced) Green's function for the source (drain) electrode and $\Sigma_{S(D)}^{\rm r(a)}$ is the retarded (advanced) self-energy of the source (drain) electrode. It can easily be shown that the coupling matrices

$$\Gamma_{S(D)} = -2\,\text{Im}\left(\Sigma_{S(D)}^{\rm r}\right), \tag{15}$$

Im represents imaginary part. The self-energies are the sum

$$\Sigma_{S(D)}^{\rm r} = \Delta_{S(D)} + i\Lambda_{S(D)}, \tag{16}$$

$\Delta_{S(D)}$ being the real part of $\Sigma_{S(D)}^{\rm r}$ corresponds to the shift of the energy levels of DNA and the imaginary part $\Lambda_{S(D)}$ is liable for the broadening of these levels.

The two-terminal Landauer conductance, at absolute zero temperature, is given by

$$g = \frac{2e^2}{h} T(E_F), \tag{17}$$

and the current passing through the system for an applied bias voltage V can be written as

$$I(V) = \frac{2e}{h} \int_{E_F - eV/2}^{E_F + eV/2} T(E) dE, \tag{18}$$

where the Fermi energy E_F is set at $E_F = 0$ eV. Here we assumed that the entire voltage drop occurs only at the boundaries of the conductor. The electronic density of states (DOS) of the system can also be obtained using the Green's function formalism. The DOS can be expressed as

$$\rho(E) = -\frac{1}{\pi} \mathrm{Im}[\mathrm{Tr}[G(E)]], \tag{19}$$

where $G(E) = (E - H_{\mathrm{DNA}} + i\eta)^{-1}$ is the Green's function for the entire DNA molecule with electron energy E as $\eta \to 0^+$, H_{DNA} is the Hamiltonian of DNA, and Im and Tr, respectively, represent the imaginary parts and trace over the entire Hilbert space.

III. RESULTS AND DISCUSSION

In Fig. 1 we plot the local density of states (LDOS) for the three DNA sequences, at zero disorder to get an idea about the density profile of the available states. We observe a band gap at the center of the band for all three sequences. This gap can be controlled via backbone energetics as reported in Ref. [28]. This LDOS profile will help us later understand the localization behavior of ds-DNA. We use the sequence "AGAAGAGAGGAAGGAGAAAGGGGGGGAAAG" for random DNA. The same for the other strand can be obtained by following complimentary base-pairing.

Let us now proceed to study the localization properties of the different DNA sequences. To perform the localization study, we define the localization length, l, as the inverse of the Lyapunov exponent γ [29], i.e.,

$$\gamma = 1/l = -\lim_{L\to\infty} \frac{1}{L} \langle \ln[T(E)] \rangle, \tag{20}$$

where L is the length of the DNA chain in terms of base pairs and $\langle \ \ \rangle$ denotes the average over different disorder configurations. In the numerical calculations we set $L = 30$ in units of base pairs. Although various distribution functions, e.g., Gaussian or binary, have been used to simulate experimental effects in previous studies [21], we think that it is appropriate to employ the most disordered case to simulate the actual experimental complications: We assume the on-site energies of backbone sites ϵ_b to be randomly distributed in the range $[-w/2, w/2]$, where w represents the backbone disorder strength.

For the numerical calculations, the on-site energies of nucleotides ϵ_{ij} are taken as the ionization potentials and the following numerical values are used in our work: $\epsilon_G = 8.177$ eV, $\epsilon_C = 9.722$ eV, $\epsilon_A = 8.631$ eV, and $\epsilon_T = 9.464$ eV.

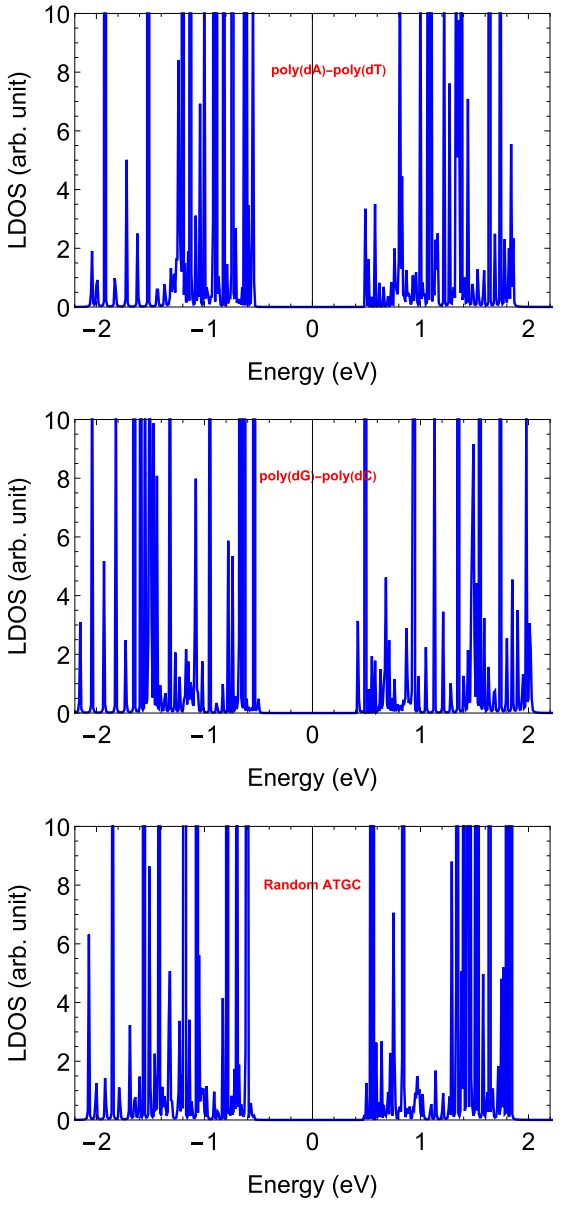

FIG. 1. LDOS, in arbitrary units, versus energy (eV) for three DNA sequences at $w = 0$. A band gap exists in all three cases at the center of the band.

These parameters are taken from the first-principle calculations [30,31]. The nearest-neighbor hopping parameter in a given strand is taken as $t_{1j} = 0.35$ eV for like bases and $t_{1j} = 0.17$ for different bases [28]. We take the interstrand hopping parameter, i.e., vertical hopping to be $v = 0.035$ eV [17], one order of magnitude smaller than the intrastrand hopping. Though there are a lot of variations available in the literature for hopping parameter values [32], we followed a specific set of previous studies as a reference as cited above.

For calculations of long-range hopping we utilize parameters arising due to helical symmetry of DNA. Specifically, we use the following parameters: $l_{1j} = 4.1$, $l_{2j} = 5.8$, $l_{3j} = 5.1$, $l_{4j} = 6.2$, $l_{5j} = 8.9$, $l_{6j} = 10.0$, and $l_c = 0.9$, all units are in Å. Using these values we can calculate the related hopping integrals t_{nj}. This procedure gives $t_{2j} \sim 0.16 t_{1j}$ and so on. It is

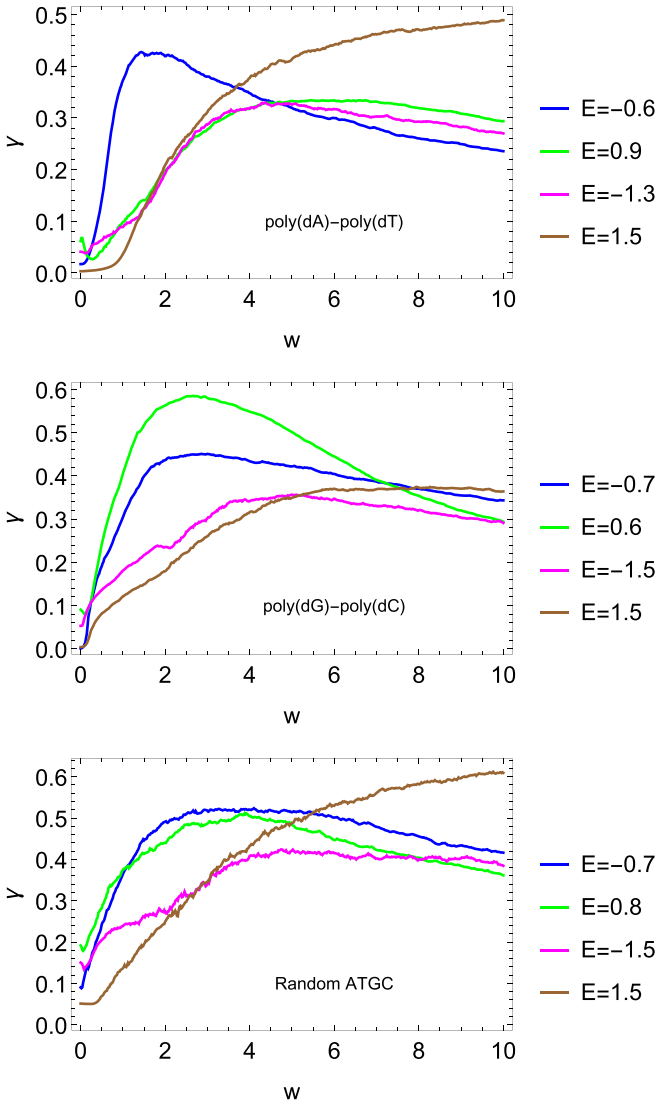

FIG. 2. Inverse localization length γ versus disorder w for the three DNA sequences at different energy values. The presence of disorder-induced delocalization is clearly visible in all three cases. Both energy (E) and disorder (w) are in eV.

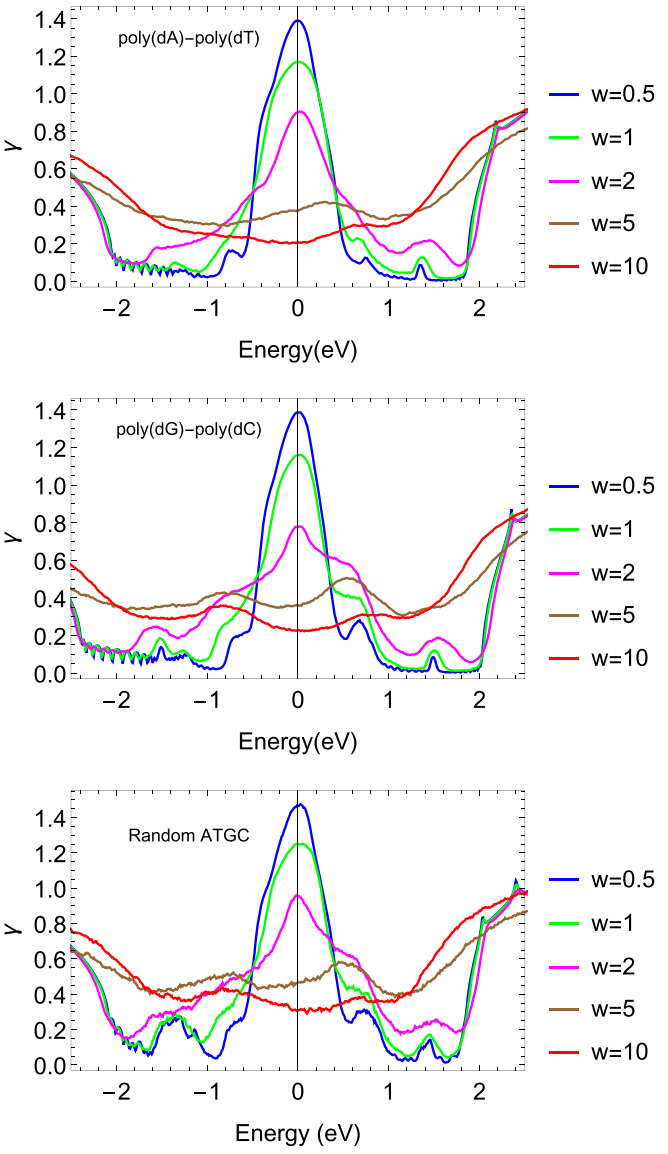

FIG. 3. Inverse localization length γ versus energy (eV) for three DNA sequences at different disorder strengths w. Both energy (E) and disorder (w) are in eV.

clear that gradually t_{nj} values will decrease (except $t_{3j} > t_{2j}$) with increasing distance, therefore we restrict ourselves up to t_{6j} and set $t_{1j} = 0.35$ eV. These parameter values for l_{nj} and t_{nj} are adopted from Refs. [13,25]. The hopping between a nucleotide and corresponding backbone is taken as $t_b = 1$ eV. We chose this value as a compromise between values found in the literature [4,17,33,34].

Numerical calculations for the inverse localization length γ versus disorder w, at different energies, are shown in Fig. 2. These energy values are taken on both sides of the band. One can see from this figure that in all the cases γ increases up to a certain value of w, and then starts decreasing. This phenomenon is known as disorder-induced delocalization. Based on the structural variability of DNA, many forms of disorder have been studied in the past (Refs. [35,36]), e.g., diagonal disorder (modification of the on-site energies of bases or base pairs) and nondiagonal disorder (modification of the interaction integrals between bases or base pairs). However, in ds-DNA, environmental effects mostly modify the energetic of sugar-phosphate backbones, so the disorder in a computational model becomes mainly off-diagonal in nature. Therefore, we ignored diagonal disorder (Anderson-like) in our present calculations. Hence, we observe that localization length starts increasing at higher values of disorder instead of decreasing.

In Fig. 3 we show the variation of γ with energy E at different disorder strength w, for the three sequences. We observe that the behavior of γ is not uniform along all energy values. As we showed in Fig. 1, there is gap at the middle of the band. With increasing disorder, some states are created in this region, which results in increasing localization length. For the rest of the energy range, γ behaves normally with disorder.

In Fig. 4 we plot the variation of transmission probability $T(E)$ for the three different DNA sequences, at multiple disorder strengths w. With increasing disorder strength, $T(E)$

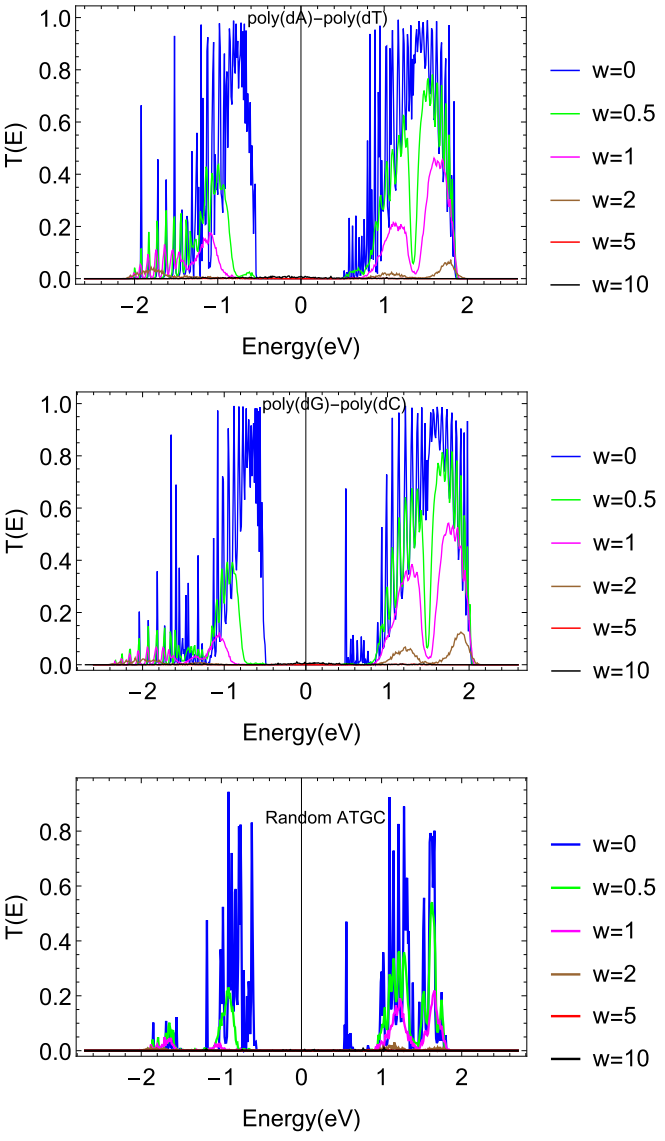

FIG. 4. Transmission probability $T(E)$ versus energy (eV) for all the DNA sequences at different disorder strengths (w). Disorder (w) has units of eV.

decreases and at very strong disorder ($w = 10$) there is no longer ballistic transport present in the system.

In Fig. 5 we depict the current-voltage (I-V) response of all DNA sequences at different disorder strength. We set the temperature at 0 K. To minimize the contact effects we choose the tunneling parameter between ds-DNA and the electrodes to be optimum, i.e., $\tau = \sqrt{t_{1j} \times t}$ [37], where t is the hopping parameter for the electrodes. One can see that, at the clean case ($w = 0$), the sequences are semiconducting in nature with their cutoff voltage around 1 V. Increasing disorder, the cutoff voltage increases and at strong disorder the sequences behave as insulators. In previous experimental studies, it was found that DNA behaves differently; some experiments reported metallic, some insulating, and some semiconducting behavior. Here we have been able to show that depending on the environmental effects, DNA can undergo a phase transition from semiconducting to insulating, which may explain different experimental findings [38–44].

In Fig. 6 we present I-V responses of a double-stranded DNA, modeled without helical symmetry and long-range hopping. In the absence of helical symmetry and long-range hopping, current outputs for all sequences drop significantly as soon as disorder is applied. If we compare Fig. 5 with Fig. 6, it becomes clear that, in the presence of multichannel transport, the current output is increased and the effect of environmental fluctuations is decreased. In a different system, namely, helical oligo-quinolinecarboxamide foldamers organized as single monolayers on Au or SiO_2, it was reported that the presence of various pathways enhances charge transport [45]. Overall, we can say the presence of helical symmetry and multiple conduction channels make charge transport through DNA more robust and make it a strong contender for future nanoelectronic devices.

IV. CONCLUSION

In the tight-binding modeling of DNA, usually helical symmetry as well as the possibility of associated extra hopping channels are ignored. Recent CISS studies with DNA and proteins [13–15] proved that the helical nature of ds-DNA gives rise to multiple conduction channels (MCC) which results in spin-polarization. In case of single-helical proteins [46], it was reported that the presence of MCCs can help in mitigating environmental effects on charge transport in a better way than in a single-stranded DNA (where MCCs are not present). In this work, we incorporated the same into ds-DNA. Our investigations show that, due to the helical symmetry and the presence of MCCs, the transport properties of DNA can be quite robust. This long-range hopping can bypass many of the environmental effects and can help in designing better DNA-based devices and wires by minimizing external disturbances.

Second, we showed that, depending on the environmental effects, DNA can undergo a phase transition from

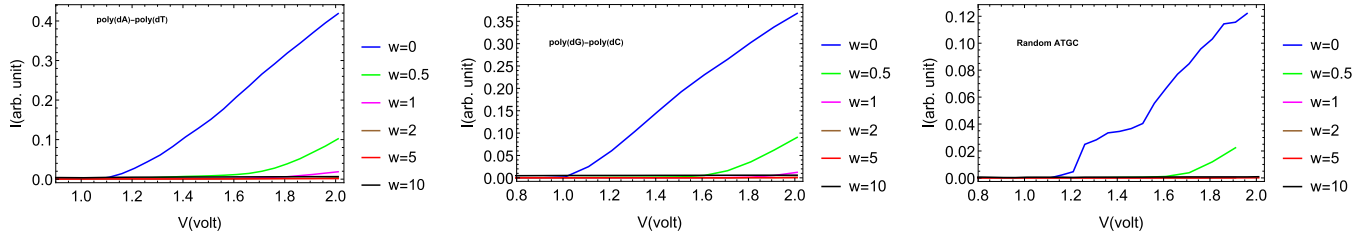

FIG. 5. I-V characteristics for ds-DNA sequences with varying disorder strength. All sequences behave almost identically; they undergo a phase transition from semiconducting to insulating with increasing disorder. Disorder (w) is expressed in eV units.

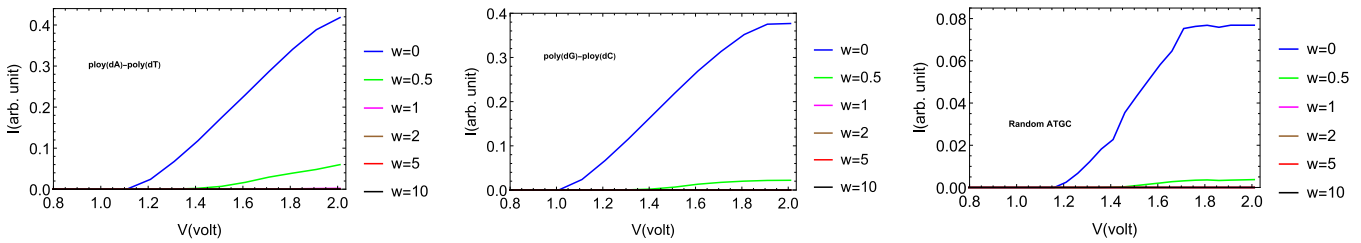

FIG. 6. *I-V* characteristics for ds-DNA sequences with varying disorder strength without helical symmetry and long-range hopping (similar to DBLM). Current outputs for all sequences drop significantly as soon as disorder is applied as compared to Fig. 5. Disorder (w) is expressed in eV units.

semiconducting to insulating. This also may solve the puzzles of many contradicting experimental findings [38–44], for example, why DNA behaves differently in transport measurements. Based on our model calculations we provided detailed insights on the behavior of ds-DNA in different environmental conditions and hope that these findings will help address the design challenges for DNA-based nanotechnology devices and components.

[1] J. Watson and F. Crick, Nature (London) **171**, 737 (1953).
[2] S. Roche, Phys. Rev. Lett. **91**, 108101 (2003).
[3] R. Gutiérrez, S. Mohapatra, H. Cohen, D. Porath, and G. Cuniberti, Phys. Rev. B **74**, 235105 (2006).
[4] G. Cuniberti, L. Craco, D. Porath, and C. Dekker, Phys. Rev. B **65**, 241314(R) (2002).
[5] J. Zhong, in *Proceedings of the 2003 Nanotechnology Conference*, Vol. 2., edited by M. Laudon and B. Romamowicz (Computational Publications, Cambridge, MA, 2003), pp. 105–108.
[6] A. K. Bakhshi, P. Otto, J. Ladik, and M. Seel, Chem. Phys. **108**, 215 (1986).
[7] J. Ladik, M. Seel, P. Otto, and A. K. Bakhshi, Chem. Phys. **108**, 203 (1986).
[8] G. Cuniberti, E. Maciá, A. Rodriguez, and R. A. Römer, in *Charge Migration in DNA: Perspectives from Physics, Chemistry and Biology*, edited by T. Chakraborty (Springer-Verlag, Berlin, 2007).
[9] S. Kundu and S. N. Karmakar, AIP Adv. **5**, 107122 (2015).
[10] M. R. Singh, J. Biomater. Sci. **15**, 1533 (2004).
[11] M. R. Singh, G. Bart, and M. Zinke-Allmang, Nanoscale Res. Lett. **5**, 501 (2010).
[12] G. P. Triberis, C. Simserides, and V. C. Karavolas, J. Phys.: Condens. Matter **17**, 2681 (2005).
[13] A.-M. Guo and Q.-F. Sun, Proc. Natl. Acad. Sci. (USA) **111**, 11658 (2014).
[14] D. Mishra, T. Z. Markus, R. Naaman, M. Kettner, B. Göhler, H. Zacharias, N. Friedman, M. Sheves, and C. Fontanesi, Proc. Natl. Acad. Sci. USA **110**, 14872 (2013).
[15] O. Ben Dor, S. Yochelis, S. P. Mathew, R. Naaman, and Y. Paltiel, Nat. Commun. **4**, 2256 (2013).
[16] T.-R. Pan, A.-M. Guo, and Q.-F. Sun, Phys. Rev. B **92**, 115418 (2015).
[17] S. Kundu and S. N. Karmakar, Phys. Lett. A **379**, 1377 (2015).
[18] G. Cuniberti, E. Maciá, A. Rodríguez, R. A. Römer, Tight-Binding Modeling of Charge Migration in DNA Devices, in *Charge Migration in DNA: Perspectives from Physics, Chemistry, and Biology*, edited by T. Chakraborty (Springer, Berlin, 2007), pp. 1–20.
[19] K. Lambropoulos, M. Chatzieleftheriou, A. Morphis, K. Kaklamanis, M. Theodorakou, and C. Simserides, Phys. Rev. E **92**, 032725 (2015).
[20] K. Lambropoulos, M. Chatzieleftheriou, A. Morphis, K. Kaklamanis, R. Lopp, M. Theodorakou, M. Tassi, and C. Simserides, Phys. Rev. E **94**, 062403 (2016).
[21] D. Klotsa, R. A. Römer, and M. S. Turner, Biophys. J. **89**, 2187 (2005).
[22] C. Simserides, A. Orfanaki, N. Margariti, and K. Lambropoulos, Materials **16**, 3200 (2023).
[23] A.-M. Guo, S.-J. Xiong, Z. Yang, and H.-J. Zhu, Phys. Rev. E **78**, 061922 (2008).
[24] C. J. Páez, P. A. Schulz, N. R. Wilson, and R. A. Römer, New J. Phys. **14**, 093049 (2012).
[25] S. Sarkar and S. K. Maiti, J. Phys.: Condens. Matter **32**, 505301 (2020).
[26] S. Datta, *Electronic Transport in Mesoscopic Systems* (Cambridge University Press, Cambridge, MA, 1995).
[27] D. S. Fisher and P. A. Lee, Phys. Rev. B **23**, 6851 (1981).
[28] S. Kundu and S. N. Karmakar, Phys. Rev. E **89**, 032719 (2014).
[29] M. Di Ventra, *Electrical Transport in Nanoscale System* (Cambridge University Press, Cambridge, MA, 2008).
[30] Y. J. Yan and H. Y. Zhang, J. Theor. Comput. Chem. **1**, 225 (2002).
[31] K. Senthilkumar, F. C. Grozema, C. F. Guerra, F. M. Bickelhaupt, F. D. Lewis, Y. A. Berlin, M. A. Ratner, and L. D. A. Siebbeles, J. Am. Chem. Soc. **127**, 14894 (2005).
[32] T. Cramer, S. Krapf, and T. Koslowski, J. Phys. Chem. C **111**, 8105 (2007).
[33] E. Macia, Phys. Rev. B **74**, 245105 (2006).
[34] E. Macia and S. Roche, Nanotechnology **17**, 3002 (2006).
[35] M. Mantela, C. Simserides, R. Di Felice, Materials **14**, 4930 (2021).

[36] M. Mantela, A. Morphis, K. Lambropoulos, C. Simserides, and R. Di Felice, J. Phys. Chem. B **125**, 3986 (2021).
[37] E. Macia, F. Triozon, and S. Roche, Phys. Rev. B **71**, 113106 (2005).
[38] H. W. Fink and C. Schönenberger, Nature (London) **398**, 407 (1999).
[39] D. Porath, S. De Vries, and C. Decker, Nature (London) **403**, 635 (2000).
[40] L. Cai, H. Tabata, and T. Kawai, Appl. Phys. Lett. **77**, 3105 (2000).
[41] P. Tran, B. Alavi, and G. Grüner, Phys. Rev. Lett. **85**, 1564 (2000).
[42] Y. Zhang, R. H. Austin, J. Kraeft, E. C. Cox, and N. P. Ong, Phys. Rev. Lett. **89**, 198102 (2002).
[43] A. J. Storm, J. van Noort, S. de Vries, and C. Dekker, Appl. Phys. Lett. **79**, 3881 (2001).
[44] K. H. Yoo, D. H. Ha, J.-O. Lee, J. W. Park, J. Kim, J. J. Kim, H.-Y. Lee, T. Kawai, and H. Y. Choi, Phys. Rev. Lett. **87**, 198102 (2001).
[45] A. Méndez-Ardoy, N. Markandeya, X. Li, Y.-T. Tsai, G. Pecastaings, T. Buffeteau, V. Maurizot, L. Muccioli, F. Castet, I. Huc, and D. M. Bassani, Chem. Sci. **8**, 7251 (2017).
[46] S. Kundu and S. N. Karmakar, Phys. Lett. A **380**, 2395 (2016).